Langmuir

Article

pubs.acs.org/Langmuir

Poly(*N*-isopropylacrylamide)-Stabilized Gold Nanoparticles in Combination with Tricationic Branched Phenylene-Ethynylene Fluorophore for Protein Identification

Keerati Kusolkamabot,[†,‡] Pornpen Sae-ung,[§] Nakorn Niamnont,[∥] Kanet Wongravee,[⊥] Mongkol Sukwattanasinitt,[#] and Voravee P. Hoven*[,#]

[†]Program in Petrochemistry and Polymer Science, Faculty of Science, Chulalongkorn University, Phayathai Road, Pathumwan, Bangkok 10330, Thailand

[‡]Center of Excellence on Petrochemical and Materials Technology, Chulalongkorn University, Phayathai Road, Pathumwan, Bangkok 10330, Thailand

[§]Program in Macromolecular Science, Faculty of Science, Chulalongkorn University, Phayathai Road, Pathumwan, Bangkok 10330, Thailand

[∥]Department of Chemistry, Faculty of Science, King Mongkut's University of Technology Thonburi, Pracha-Uthit Road, Thung Khru, Bangkok 10140, Thailand

[⊥]Sensor Research Unit, Department of Chemistry, Faculty of Science, Chulalongkorn University, Phayathai Road, Pathumwan, Bangkok 10330, Thailand

[#]Organic Synthesis Research Unit, Department of Chemistry, Faculty of Science, Chulalongkorn University, Phayathai Road, Pathumwan, Bangkok 10330, Thailand

Supporting Information

ABSTRACT: Gold nanoparticles stabilized by thermoresponsive polymer, poly(*N*-isopropylacrylamide) (PNIPAM-AuNPs) were prepared by surface grafting of thiol-terminated PNIPAM onto citrate-stabilized AuNPs. The color change of the PNIPAM-AuNPs solution from red to blue-purple without precipitation when the solution was heated to 40 °C, above the lower critical solution temperature (LCST) of PNIPAM, indicated the thermoresponsive property of the synthesized AuNPs. PNIPAM-AuNPs were used to detect proteins by chemical nose approach based on fluorescence quenching of fluorophore by AuNPs. An array-based sensing platform for detection of six proteins, namely bovine serum albumin, lysozyme, fibrinogen, concanavalin A, hemoglobin, holo-transferrin human can be successfully developed from the PNIPAM-AuNPs having different molecular weights (4 and 8 kDa) and conformation (varied heat treatment from 25 to 40 °C) in combination with a tricationic branched phenylene-ethynylene fluorophore. From principal component analysis (PCA) followed by linear discriminant analysis (LDA), 100% accuracy of protein classification using a leave-one-out (LOO) approach can be achieved by using only two types of PNIPAM-AuNPs.

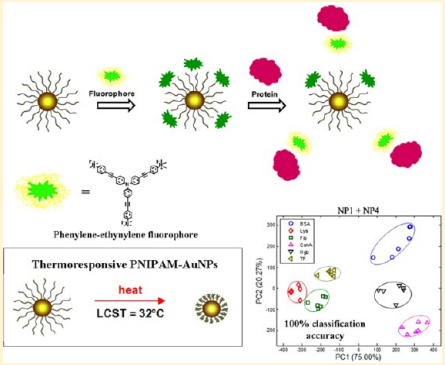

INTRODUCTION

Gold nanoparticles (AuNPs) have been the focus of considerable interest due to their potential applications for catalysis, diagnosis, and photoelectronic devices. Highly dispersed AuNP solutions exhibit a red color with an absorption band around 520 nm due to the excitation of surface plasmon by incident light. The association of the AuNPs dispersed in the solution induces a color change from red to blue-purple, which can be applied for the development of colloidal sensors.[1−3] Considerable effort has been devoted to synthesis of AuNPs, focusing on control over their size, shape, solubility, stability, and functionality. In general, AuNPs in solution are susceptible to aggregation themselves. To improve their dispersibility and introduce functionality to particle surfaces, the AuNPs may be coated with a water-soluble polymer having a functionality that can interact with gold. It has been reported that some polymers are effective stabilizing agents because they are capable of providing both electrostatic and steric stabilizations to the gold particles.[4,5]

Intelligent polymers, also known as "stimuli-responsive" or "environmentally sensitive" polymers,[6−9] can undergo relatively large and abrupt, physical, or chemical changes in response to small external stimuli in the environmental conditions.[10−13] One of the most recognizable polymers in the class is poly(*N*-

Received: June 5, 2013
Revised: August 22, 2013
Published: August 23, 2013

Scheme 1[a]

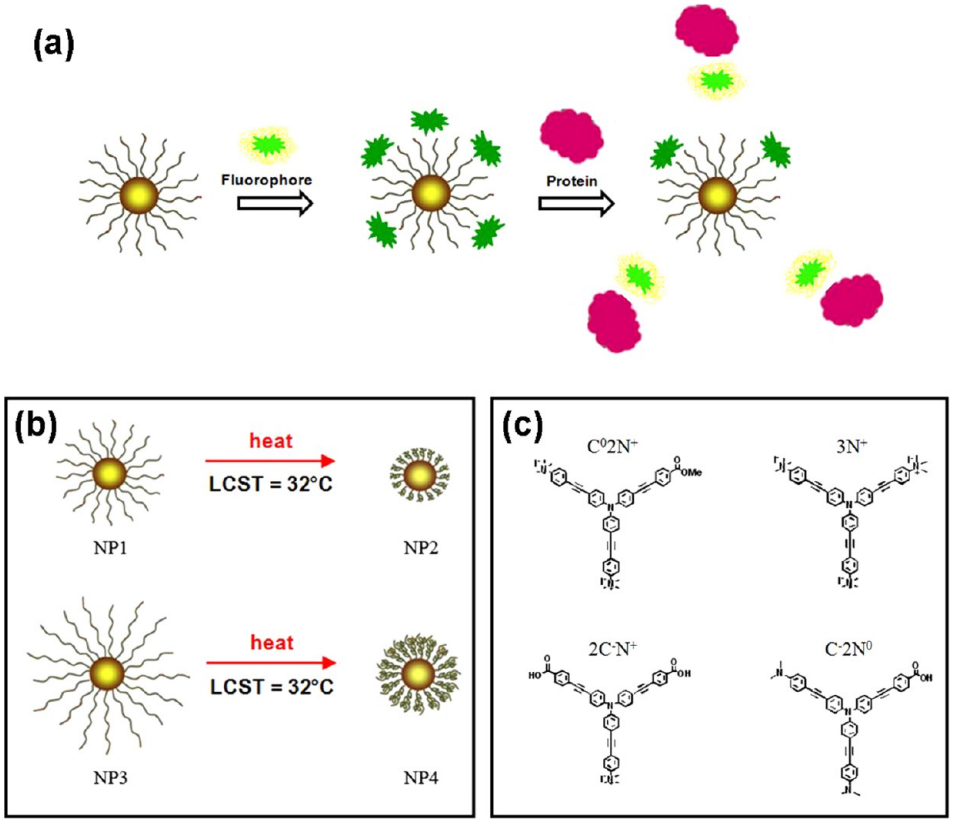

[a](a) Concept of sensor based on competitive binding of PNIPAM-AuNPs and protein with fluorophore that has an impact on fluorescence quenching, (b) four different types of PNIPAM-AuNPs (NP1-NP4), and (c) chemical structures of four tribranched phenylene-ethynylene fluorophores.

isopropylacrylamide) (PNIPAM). PNIPAM dissolves in water assuming a random coil conformation at room temperature, but it separates from the aqueous phase when heated above 31−32 °C, its lower critical solution temperature (LCST).[14−17] Such thermoresponsive behavior is also maintained for PNIPAM grafted on AuNPs (PNIPAM-AuNPs) which can be evidenced from color transition of a AuNPs aqueous solution above and below the LCST. The solution would turn from red to blue upon the collapse of extended brushlike PNIPAM chains above LCST and caused AuNPs aggregation.[18−22]

Recently, it has been reported that protein as a biomarker can be detected by chemical nose approach based on fluorescence quenching of fluorophore by functionalized AuNPs.[23−26] The binding equilibrium between fluorophore and AuNPs would be altered because of competitive binding of protein analyte. Upon an addition of protein analyte, quenched fluorophore adsorbed on the AuNPs surface can be replaced by protein resulting in the recovery of fluorescence signal from the fluorophore. The fluorescence response may be positive or negative depending on the binding affinity of protein toward AuNPs and fluorophore. Although the chemical nose approach relies very much on nonspecific interactions between protein and AuNPs, it is selective enough to be used for identifying the type of individual protein based on the variation of quenching ability of AuNPs having different functionality and the binding strength between the functionalized AuNPs and different kind of protein.[26]

Taking advantage of the PNIPAM-AuNPs being capable of undergoing thermoresponsive conformational transition of the surface-grafted PNIPAM between extended brushes to collapsed chains upon heat treatment above or below the LCST, it is anticipated that the distance between the core of AuNPs and fluorophore as well as protein in solution and so the degree of fluorescence quenching/recovery and the binding strength with the protein should be altered upon heat treatment. This would be highly beneficial if these PNIPAM-AuNPs are to be put in an array-based protein detection following chemical nose approach strategy because the other kind of AuNPs can be obtained by simply heating the existing AuNPs. Considering that PNIPAM is a polymer, such distance may also be varied as a function of PNIPAM molecular weight. In particular, reversible addition−fragmentation chain transfer (RAFT) polymerization has been well recognized as an effective controlled radical polymerization process for PNIPAM synthesis. Not only can a precise control over molecular weight and polydispersity of PNIPAM be achieved, but the terminal dithioester group at the PNIPAM chain end can also be converted to thiol group which is readily available for grafting onto the surface of gold.[27−31]

This research aims to combine the thermoresponsive behavior of PNIPAM and the fluorescence quenching properties of AuNPs to create hybrid materials to be used for protein detection, a mode of biosensing application, to the best of our knowledge, that has never been described before. Together with phenylene-ethynylene tribranched fluorophores having tunable charge characteristic, synthetic dyes successfully used for protein discrimination based on a chemical nose approach,[32] an array-based chemical nose sensor for protein

dx.doi.org/10.1021/la402139g | Langmuir 2013, 29, 12317−12327

detection was developed based on the concept of fluorescence quenching schematically described in Scheme 1a.

EXPERIMENTAL SECTION

Materials. Hydrogen tetrachloroaurate ($HAuCl_4 \cdot 3H_2O$), 4,4′-azobis(4-cyanopentanoic acid) (ACPA), 4-cyano-4-(thiobenzoylthio)-pentanoic acid (CPD), tris(2-carboxyethyl)phosphine hydrochloride (TCEP), and *N*-isopropylacrylamide (NIPAM) were obtained from Aldrich. Bovine serum albumin (BSA), lysozyme (Lys), fibrinogen (Fib), concanavalin A (Con A), hemoglobin (Hgb), holo-transferrin human (TF), dialysis bag (cut-off molecular weight of 3500 g/mol), and phosphate buffered saline pH 7.4 (PBS) were bought from Sigma. 2-Ethanolamine and trisodium citrate dihydrate ($Na_3C_6H_5O_7 \cdot 2H_2O$) were obtained from Fluka (Switzerland). The above chemicals as well as all solvents used (1,4-dioxane, tetrahydrofuran (THF), methanol (MeOH)) were analytical grade and used as received without further purification except NIPAM which was recrystallized in a mixture of benzene and *n*-hexane (3:7, v/v) prior to use. Four fluorophores ($C^0 2N^+$, $3N^+$, $2C^- N^+$, and $C^- 2N^0$) having different charges were synthesized according to a published procedure reported by Niamnont et al.[32] All solutions were prepared using ultrapure distilled water that was obtained after purification using a Millipore Milli-Q system that involves reverse osmosis, ion exchange, and a filtration step (18.2 MΩ cm resistance).

Characterization. Molecular weight of the synthesized PNIPAM was analyzed by GPC using a Waters 600 controller chromatograph equipped with HR1 and HR4 columns (Waters, MW resolving range = 100−500 000) at 35 °C and refractive index detector (Waters 2414). THF was used as eluent with a flow rate of 1.0 mL/min. Five polystyrene standards (996−188 000 Da) were used for generating a calibration curve. Fluorescence signals of the fluorophores were recorded by using a Perkin-Elmer precisely (LS 45) luminescence spectrometer (PerkinElmer Inc., UK) in a scanning wavelength range of 400−700 nm. The presence of the polymer around the AuNPs was confirmed by using a Seiko SPA 400 atomic force microscope (SII Nanotechnology Inc., Japan). Measurements were performed in air at ambient temperature using tapping mode and silicon tips with a resonance frequency of 115−190 kHz. Surface plasmon resonance (SPR) measurements used for the determination of PNIPAM coverage on gold surface were conducted using a double channel, AutoLab ESPR (Eco Chemie, Netherlands). The morphology and actual size of AuNPs were analyzed by using a JEOL JEM-2010 transmission electron microscope (Japan) operating at 80 keV. The average diameters of AuNPs were reported from measurements of 30 random particles for each sample using Semafore software. The zeta (ζ) potential of AuNPs were determined using Nanosizer Nano-ZS (Malvern Instruments, UK). The analysis was performed at 25 °C using a scattering angle of 173°. The data were calculated using the Helmholtz-Smoluchowski equation.

Synthesis of Thiol-Terminated PNIPAM (PNIPAM-SH). PNIPAM having two different target degrees of polymerization (DP = 40 and 70) were prepared by RAFT polymerization. According to a method modified from that of Yusa et al.,[19] CPD (17.5 mg, 62.5 μmol) and ACPA (8.8 mg, 31.3 μmol) were added to a NIPAM (565.8 mg, 5.0 mmol) solution in 1,4-dioxane (5 mL). The solution was degassed by purging with nitrogen gas for 30 min, and then heated at 70 °C for 24 h. After being cooled down in an ice bath, the reaction mixture was dialyzed against DI water at 4 °C for 3 days, before the PNIPAM was recovered by lyophilization. To remove the terminal dithiobenzoate group, an aqueous solution of PNIPAM was treated with 2-ethanolamine (30 mol equiv of PNIPAM) and a trace amount (3−5 mg) of TCEP at 25 °C for 24 h. The solution was dialyzed against DI water at 4 °C for 3 days. The PNIPAM-SH was then obtained after lyophilization. The condition mentioned above was used to prepare PNIPAM with targeted DP = 40 (targeted molecular weight = 4805.78 g/mol). To prepare PNIPAM with targeted DP = 70 (targeted molecular weight = 8200.58 g/mol), CPD (11.1 mg, 39.7 μmol) and ACPA (4.5 mg, 15.9 μmol) were used instead.

Preparation of AuNPs Stabilized by PNIPAM (PNIPAM-AuNPs). PNIPAM-AuNPs were prepared by surface grafting of PNIPAM-SH onto citrate-stabilized AuNPs. In the first step, citrate-AuNPs were synthesized according to a method modified from that of Hayat.[33] An aqueous solution of trisodium citrate (1% w/v, 1.75 mL) was added to a boiling aqueous solution of $HAuCl_4$ (0.01% w/v, 50 mL). Then, the mixture was heated for 30 min and cooled down to ambient temperature. At this point, the color of the solution was changed from gray to red. Finally, the synthesized AuNPs were stored at 4 °C prior to use. It should be noted that all glassware used for the synthesis of AuNPs was washed with freshly prepared aqua regia solution (HCl/HNO_3 = 3:1, v/v) and rinsed thoroughly with distilled water prior to use. PNIPAM-AuNPs were obtained by grafting to method modified from that of Zhu et al.[18] PNIPAM-SH (2.0 μmol) was dissolved in 10 mL of citrate-stabilized AuNPs solution obtained from the first step and kept at 4 °C for 48 h. After that, excess PNIPAM-SH was removed from the PNIPAM-AuNPs by centrifugation twice (MIKRO 120, Hettich, Germany) at 14 000 rpm for 15 min intervals. After redispersion in Milli-Q water, a red solution of PNIPAM-AuNPs was obtained and kept at 4 °C.

Determination of Fluorescence Quenching of Fluorophores by PNIPAM-AuNPs. Quenching efficiency of four tribranched phenylene-ethynylene fluorophores having different charges of which structures are shown in Scheme 1c was evaluated with PNIPAM-AuNPs to find the fluorophores that can be highly quenched by AuNPs. The abbreviated names of the fluorophores are assigned according to the number and types of the functional groups on their peripheries in which C^0, C^-, N^0, and N^+ stand for carboxylate ester, carboxylic acid (or carboxylate anion in basic condition), amino, and quaternary ammonium groups, respectively. For example, $C^0 2N^+$ possesses one carboxylate ester and two quaternary ammonium groups on its periphery. To determine quenching efficiency, the initial fluorescence signal of fluorophore was determined by diluting the fluorophore stock solution (10.0 μM, 100 μL) in 2.9 mL of PBS solution and measured by using a luminescence spectrometer. The quenching efficiency of PNIPAM-AuNPs was determined by mixing the fluorophore stock solution (10.0 μM, 100 μL) and 500 μL of PNIPAM-AuNPs solution in 2.4 μL of PBS solution in a cuvette. To ensure that the equilibrium was attained, the mixture was allowed to stand at ambient temperature for 30 min before the measurement of the emission spectrum.

Determination of Fluorescence Response of Fluorophore by Proteins. All of the fluorophores were tested with BSA. The selected fluorophore (10.0 μM, 100 μL) was first dissolved in 2.9 mL of PBS solution in a cuvette. After the solution was left for 30 min, the initial fluorescence emission of fluorophore was analyzed by using a luminescence spectrometer. BSA (10 μL, 1 mg/mL) was then added to the mixture obtained from the first step. To ensure that the equilibrium was attained, the mixture was analyzed by using a luminescence spectrometer after leaving for 30 min. To maximize the fluorescence quenching effect of the PNIPAM-AuNPs on the fluorophores, the fluorophores showing the least response to proteins were selected for developing a sensor platform based on the chemical nose approach.

Protein Detection Based on Fluorescence Quenching. The synthesized PNIPAM-AuNPs were put in an array-based sensing platform. Six types of proteins (BSA, Lys, Fib, Con A, Hgb, and TF) were analyzed by using four different types of PNIPAM-AuNPs having varied PNIPAM molecular weight and conformation (induced by thermal treatment) together with the selected phenylene-ethynylene fluorophore. There are four different types of PNIPAM-AuNPs used for this investigation. Two types were obtained from the AuNPs stabilized by 4 kDa of PNIPAM-SH (4k PNIPAM-AuNPs). The first type is 4k PNIPAM-AuNPs at 25 °C (NP1) which was obtained directly from the subsection "Preparation of AuNPs Stabilized by PNIPAM (PNIPAM-AuNPs)" above. The second type is 4k PNIPAM-AuNPs at 40 °C (NP2) which was obtained by heating NP1 for 15 min and cool it down to 25 °C and leave it for 30 min before conducting further experiment. Another two types were obtained from AuNPs stabilized by 8 kDa of PNIPAM-SH (8k

dx.doi.org/10.1021/la402139g | Langmuir 2013, 29, 12317−12327

PNIPAM-AuNPs). The third type is 8k PNIPAM-AuNPs at 25 °C (NP3) and the forth type is 8k PNIPAM-AuNPs at 40 °C (NP4) obtained by a similar heat treatment as mentioned above of NP3. The detection of protein was done as follows. In the first step, 0.5 mL of NP1 was dissolved in 2.4 mL of PBS. After that, $3N^+$ fluorophore (1×10^{-5} M, 100 μL) was then added and analyzed via luminescence spectrometer after 30 min allowed for the equilibrium time. The second step, BSA (10 μL, 1 mg/mL), was added to the previous mixture and analyzed via luminescence spectrometer again after the equilibrium time. BSA was subjected to the same analysis with NP2, NP3, and NP4. To generate an array-based sensing platform, other types of proteins were also tested with NP1, NP2, NP3, and NP4.

Data Analysis. All data analysis program were written in-house using MATLAB version R2011b. The software for principal component analysis (PCA) and linear discriminant analysis (LDA) was programmed using the algorithm described elsewhere.[34] In our case, LDA was not directly performed to the original data set where the number of variables (wavelengths) exceeds the number of samples as the inverse of the pooled variance-covariance matrix is impossible to be calculated.[34,35] To avoid the problem, the procedure called "PCA-LDA" was used to demonstrate the classification power.[36−38] The approach is to compress the dimension of the data into a low number of principal component (PC) using PCA and LDA is then performed on the resulting PC scores to quantify the discriminant ability.

RESULTS AND DISCUSSION

Preparation and Characterization of PNIPAM-SH. Here in this research, PNIPAM was synthesized by RAFT polymerization of which molecular weight and polydispersity can be well controlled by using a chain transfer agent. Besides, the dithioester group at the polymer chain end can be converted to a thiol group that is readily available for grafting onto the gold surface.[39] The chemical structure of the synthesized PNIPAM was verified by ^{1}H NMR (Figure S1, Supporting Information). Its characteristic signals were consistent with those reported in the literature.[40,41] As determined by ^{1}H NMR data, it was found that the percent conversion and the average M_n of PNIPAM were 41% and 4053 g/mol, and 42% and 7015 g/mol for targeted DP of 40 and 70, respectively.

Cleavage of the terminal dithiobenzoate group at the PNIPAM chain end was confirmed by UV−vis analysis. Upon aminolysis by using 2-ethanolamine, the UV absorption band around 300 nm corresponding to the dithiobenzoate group disappeared resulting in the formation of thiol group and yielded PNIPAM-SH (Figure S2 in the Supporting Information). The success of aminolysis was also confirmed by the appearance of PNIPAM which changed from pink-orange to white as a result of dithiobenzoate group removal. Since the thiol-terminated polymers can easily be oxidized by oxygen, internal disulfide linkage may be formed and possibly yielded an overestimated molecular weight. To ensure that such incidence did not occur, the molecular weights of PNIPAM-SH were also determined by GPC. The data shown in Table 1 indicated that the M_n and PDI (M_w/M_n) values of PNIPAM before aminolysis and after aminolysis (PNIPAM-SH) were closely resembled, implying that the disulfide bond formation was absent.[42] The fact that all PDI values are very close to one another verifies that the molecular weight distribution is narrow and that the RAFT polymerization is well-controlled.

Preparation and Characterization of PNIPAM-AuNPs. PNIPAM-SH obtained from the previous section was directly grafted onto the surface of AuNPs through sulfur−gold interaction. As compared with the Fourier transform infrared (FTIR) spectrum of PNIPAM (Figure S3a, Supporting Information), the FTIR spectrum of the PNIPAM-AuNPs

Table 1. Molecular Weight and Polydispersity Values of PNIPAM and PNIPAM-SH

	target					
polymer	DP	M_n	[M]/[I]/[CTA] (mmol)	M_n[a]	PDI[a]	M_n[b]
PNIPAM	40	4526	1.600/0.01/0.020	3816	1.09	4053
	70	7921	3.145/0.01/0.025	8552	1.13	7015
PNIPAM-SH	40	4526	1.600/0.01/0.020	4180	1.11	n/a
	70	7921	3.145/0.01/0.025	8788	1.14	n/a

[a]Determined by GPC analysis using THF as eluent. [b]Calculated from ^{1}H NMR data.

(Figure S3b, Supporting Information) has characteristic peaks of N−H stretching from secondary amide at 3276 cm^{-1} and C−H deformation of isopropyl groups with a 1:1 intensity ratio at 1386 and 1367 cm^{-1} which indicated the success of PNIPAM-SH coating on the surface of AuNPs.

The layer of PNIPAM shell surrounding the AuNPs can be visualized from atomic force microscopy (AFM) images shown in comparison with that of the uncoated AuNPs stabilized by citrate ions in Figure 1. In addition, the effects of molecular

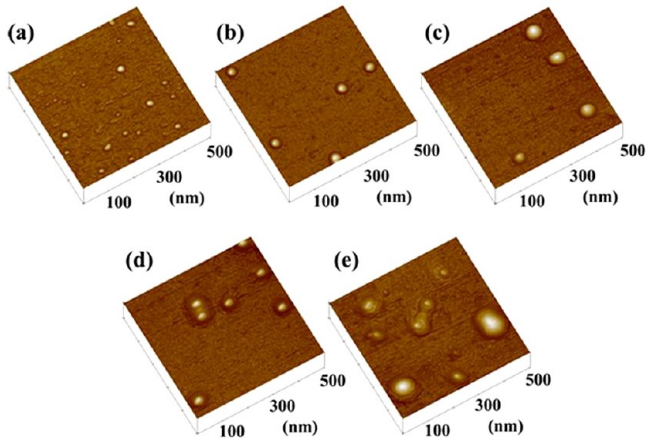

Figure 1. AFM images of (a) uncoated citrated-stabilized AuNPs and AuNPs coated with (b) 0.2 mM 4k PNIPAM-SH, (c) 0.2 mM 8k PNIPAM-SH, (d) 0.5 mM 4k PNIPAM-SH, and (e) 0.5 mM 8k PNIPAM-SH.

weight and concentration of PNIPAM-SH on grafting efficiency were investigated. Apparently, the uncoated AuNPs were smaller than all of the PNIPAM-AuNPs. For the AuNPs surrounded by PNIPAM-SH, the particle size was increased with elevating molecular weight of PNIPAM (from 4 to 8 kDa). As illustrated in Figure 1d and e, the expansion of shell thickness was also evidenced as a function of PNIPAM-SH concentration. It was found that the proper concentration of PNIPAM-SH was 0.2 mM because it was the minimum concentration that still gave AuNPs with thermoresponsive property which can be realized from color transition of the AuNPs solution upon thermal treatment, the detail of which will be described in the following section. Moreover, the grafting quantity of the two PNIPAM-SH having different molecular weights (4 and 8 kDa) on a flat gold surface was determined by using SPR analysis (detailed experimental procedure is included along with the data shown in Table S1 in the Supporting Information). Apparently, 4k PNIPAM could

dx.doi.org/10.1021/la402139g | Langmuir 2013, 29, 12317−12327

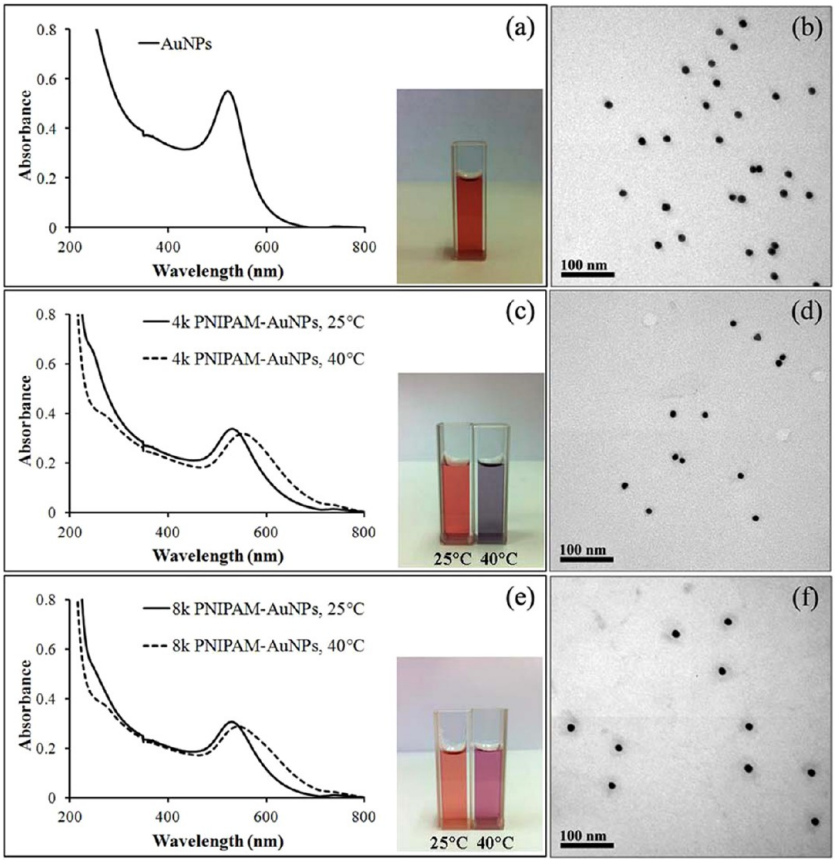

Figure 2. UV−vis spectra (a,c,e) and TEM images (b,d,f) of citrated-stabilized AuNPs (a,b), 4k PNIPAM-AuNPs (c,d), and 8k PNIPAM-AuNPs (e,f). The insets of (c) and (e) show the color transition of PNIPAM-AuNPs solution upon heating from 25 to 40 °C.

be grafted with higher density and more consistently than 8k PNIPAM.

The surface plasmon band of AuNPs is known to be sensitive to the size of the particles and their surrounding environment. As demonstrated in Figure 2a, a solution of highly dispersed citrated-stabilized AuNPs exhibits red color with an absorption band around 520 nm. According to transmission electron microscopy (TEM) analysis, the particles were spherical in shape and showed uniform size distribution around 13 nm (Figure 2b). In principle, PNIPAM chains should be collapsed upon increasing temperature above its LCST of 32 °C which is a consequence of hydrogen bonding between water and PNIPAM being destroyed at elevated temperature. Figure 2c shows UV−vis absorption spectra of 4k PNIPAM-AuNPs at 25 °C (NP1) and 40 °C (NP2) in PBS solution. The absorption maximum of the plasmon band of 530 nm at 25 °C shifted to 551 nm when the temperature was increased to 40 °C. The color of the solution changed from red to blue-purple (from NP1 to NP2) without precipitation. The particles were still spherical in shape and consisted of 13 nm gold core and 1 nm PNIPAM shell, as can be seen in the TEM image (Figure 2d). Figure 2e shows UV−vis absorption spectra of 8k PNIPAM-AuNPs at 25 °C (NP3) and 40 °C (NP4) in PBS solution. The absorption maximum of the plasmon band of 530 nm at 25 °C only slightly shifted to 541 nm after heating to 40 °C. This slight red shift might be attributed to a high thickness of PNIPAM shell which prevented an aggregation of the AuNPs. This result was consistent with the color of the solution in that the solution was altered from red to pink-purple (from NP3 to NP4) without precipitation. It was found that the particles were spherical in shape with well-defined core/shell nanostructures having 13 nm gold core and 14−17 nm PNIPAM shell (Figure 2f). The data depicted in Table S2 in the Supporting Information also suggested that the relative dimension of the particles measured by AFM was larger than those analyzed by TEM. This may be ascribed to the fact that AFM analysis was performed under semidried conditions.

It should also be emphasized that the thermoresponsive property upon this thermal treatment condition is not reversible. The solution color as well as absorption maxima of plasmon bands of both NP2 and NP4 remained unaltered although their solutions were quenched down to ambient temperature (25 °C) for a long period of time (up to 2 h), implying that both NP2 and NP4 maintained at their aggregated states and did not turn back to their original NP1 and NP3, respectively, at least within the period of measurements. This irreversibility is not completely unknown. In fact, it has been previously reported on the system of magnetic nanoparticles coated with PNIPAM-containing copolymers having relatively low graft density.[43] Our PNIPAM-AuNPs were prepared by grafting-to method so their graft density may not be that high which could be the reason of their irreversible thermal transition.

It has also been reported by Yusa et al.[19] that the thermoresponsive property of PNIPAM-AuNPs in terms of color transition (shift in absorption maximum of surface plasmon band) cannot be observed unless salt was added. They have explained that the color transition, in principle, should be driven by both PNIPAM shrinkage upon heating above its LCST and interparticle aggregation of the PNIPAM-AuNPs.

dx.doi.org/10.1021/la402139g | Langmuir 2013, 29, 12317−12327

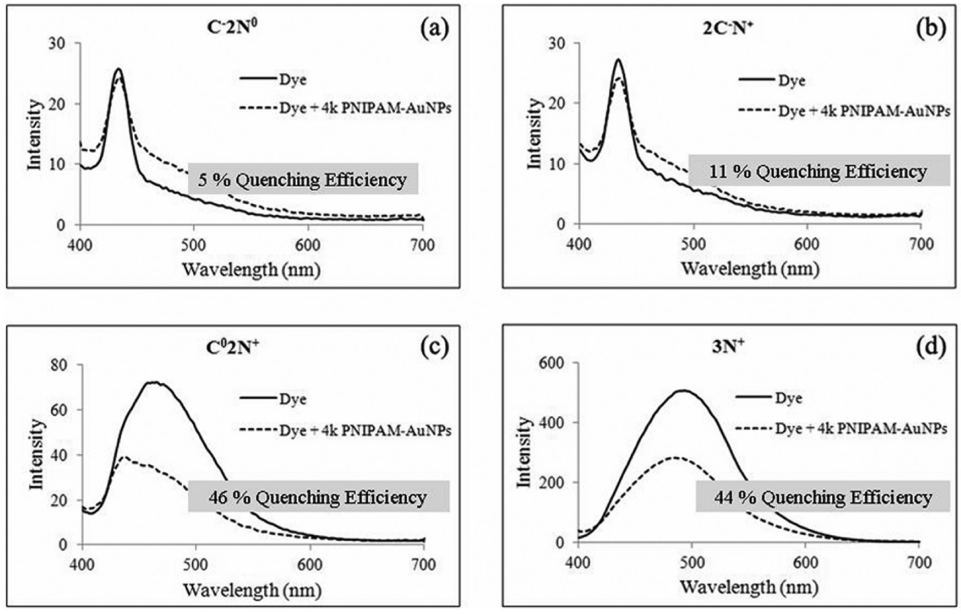

Figure 3. Emission spectra demonstrating quenching behavior of four phenylene-ethynylene fluorophores: (a) $C^{-}2N^{0}$, (b) $2C^{-}N^{+}$ (c) $C^{0}2N^{+}$, and (d) $3N^{+}$ by using 4k PNIPAM-AuNPs (NP1) as a quencher.

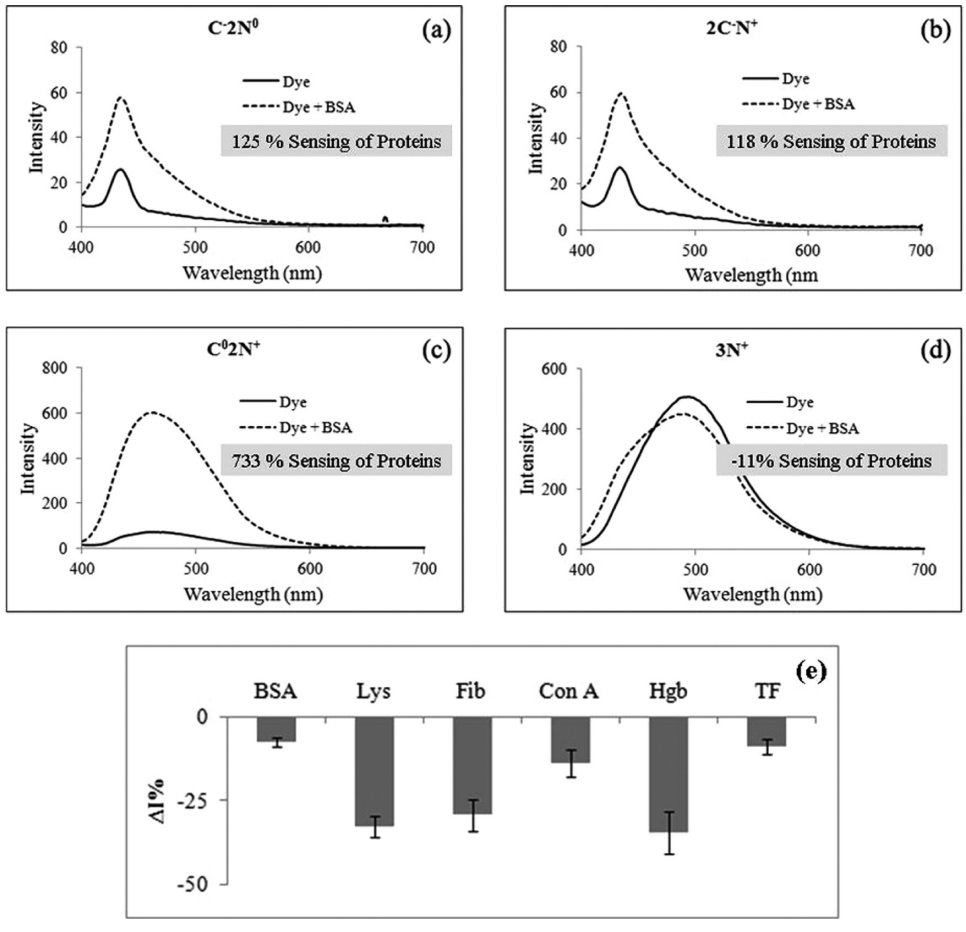

Figure 4. Emission spectra demonstrating the change in fluorescence intensity of four tribranched phenylene-ethynylene fluorophores: (a) $C^{-}2N^{0}$, (b) $2C^{-}N^{+}$, (c) $C^{0}2N^{+}$, and (d) $3N^{+}$ upon BSA addition, and (e) percentage of the change in emission intensity of $3N^{+}$ fluorophore when tested with six proteins.

Thermal treatment above LCST should cause PNIPAM shrinkage (which can be realized by change in hydrodynamic radius usually determined by light scattering), however, the thermal energy is apparently not enough to bring together the collapsed PNIPAM-AuNPs that should lead to aggregation and subsequent change in optical characteristic (color change). This

dx.doi.org/10.1021/la402139g | *Langmuir* 2013, 29, 12317−12327

may be rationalized as a consequence of strong hydrogen bonding between water and the PNIPAM particularly at the outer layer of the PNIPAM-AuNPs that prevent aggregation. Introducing salt to the system helped increasing ionic strength so that such strong hydrogen bonding can be destroyed and allows the aggregation to take place. For this reason, we also conducted additional experiments by incorporating 50 mM NaCl to the PNIPAM-AuNPs solution and performed two cycles of heating-quenching between 25 and 40 °C and found that the color transition from red to blue-purple can be promptly accelerated and the process was also reversible as can be demonstrated in Figure S4 (Supporting Information). Such results have suggested that whether the visible thermoresponsiveness is reversible truly depends on the solution properties (i.e., ionic strength).

In this research, it is our intention not to add any salt to the solution which may complicate the protein classification that relies on the interactions among three counterparts (PNIPAM-AuNPs, fluorophore, and protein). For this reason, the thermoresponsive transition solely relied on thermal energy introduced to the system by heating. The thermoresponsiveness of the PNIPAM-AuNPs was not reversible which was presumably caused by the relatively low graft density of the PNIPAM as mentioned above. On the other hand, it was also possible that prolonged heating (>15 min in this research) caused extensive PNIPAM collapse and dehydration, making interparticle aggregation a permanent process. Nevertheless, the irreversibility is truly beneficial for the mode of detection proposed in this research work in that both NP2 and NP4 maintained their optical characteristic throughout the experiment, suggesting that the method is reliable.

Protein Identification. To put the synthesized PNIPAM-AuNPs in an array-based sensing platform, a preliminary investigation on quenching efficiency of four tribranched phenylene-ethynylene fluorophores having different charges (structure shown in Scheme 1c) by 4k PNIPAM-AuNPs at 25 °C was performed. It should be emphasized that these specific fluorophores were chosen because their charge characteristic can be tuned by varying the peripheral groups of the branch in the fluorophore structure without affecting their size. This is beneficial from the point that the impact of the charge on the quenching/recovery of the fluorophore can be determined without having to be concerned about the size and dimension variation of the fluorophore. As presented in Figure 3, when 4k PNIPAM-AuNPs were used as a quencher, the $C^{-}2N^{0}$ and $2C^{-}N^{+}$ fluorophores were slightly quenched (5% and 11%, respectively), while the $3N^{+}$ and $C^{0}2N^{+}$ fluorophores were largely quenched (44% and 46%, respectively). The $C^{-}2N^{0}$ fluorophore has one carboxylic acid and two amino groups providing −1 net electronic charge, whereas the $2C^{-}N^{+}$ fluorophore has two carboxylic acid groups and one quaternary ammonium group also netting −1 electronic charge. Therefore, there should be the repulsive force between the fluorophores and PNIPAM-AuNPs which have lone paired electrons of nitrogen and oxygen in the repeating unit resulting in ineffective fluorescence quenching. On the other hand, $3N^{+}$and $C^{0}2N^{+}$ fluorophores have +3 and +2 net electronic charges. As a result, the electrostatic attraction between these positively charged fluorophores and PNIPAM-AuNPs yielded more effective quenching. For this reason, only $3N^{+}$ and $C^{0}2N^{+}$ fluorophores were selected for further investigation. Furthermore, to ensure that the fluorescence response would originate from quenching by the PNIPAM-AuNPs, the interactions between the fluorophore and protein were investigated. In principle, the fluorophore having the least response with proteins is more desirable to be used for the development of protein sensor based on our designed fluorescence quenching.

As can be seen in Figure 4, the emission intensity of $3N^{+}$ fluorophore was minimally affected by BSA. Therefore, $3N^{+}$ fluorophore was selected for further investigation. The much lower fluorescence response of $3N^{+}$ toward BSA than that previously reported by Niamnont and co-workers[32] could be described as a result of the protein concentration used in this research (3.3 μg/mL having A_{280} = 0.0028) being lower than that (A_{280} = 0.01) used in the previous work. Such lower protein concentration used in this sensing system was presumably not high enough for the BSA to act as effective surfactant that help deaggregating the fluorophore ($3N^{+}$) which should lead to fluorescence signal enhancement, the principle determined quenching efficiency described in their work. Nevertheless, we find this as a potential benefit given that the fluorescence response of $3N^{+}$ is more sensitive to lower protein concentration when used in combination with PNIPAM-AuNPs. To confirm that the $3N^{+}$fluorophore was a proper dye, it was also tested with other five different types of protein having different pI and MW (Lys, Fib, Con A, Hgb, and TF) and was found that all types of proteins did not enhance fluorescence intensity of $3N^{+}$ (Figure 4e).

To study the effect of polymer conformation grafted on AuNPs surface on the quenching efficiency, NP1 and NP2 were compared and found that the quenching efficiency of NP2 was higher than that of NP1 (Figure S5 in the Supporting Information). This may be because the conformation of PNIPAM changed from stretched to coil-like structure upon heating to above its LCST, resulting in the decreasing of distance between the gold core of NP2 and the fluorophore that in turn enhanced the quenching efficiency. To determine the effect of polymer molecular weight grafted on AuNPs surface on the quenching efficiency, NP1 and NP3 were compared. It was found that the quenching efficiency of NP1 was greater than that of NP3. This may be explained as a result of the PNIPAM layer on the NP1 being thinner than that on the NP3. The closer distance between the gold core and fluorophore in the case of NP1 when compared to that of the NP3 thus promotes the quenching process. The data shown in Table S3 in the Supporting Information demonstrated that all PNIPAM-AuNPs initially possessed negative zeta potential values, all of which became less negative upon $3N^{+}$ addition. These evidently supported the assumption that the quenching was driven by electrostatic attraction between the positive charge of the $3N^{+}$ fluorophore and the lone paired electrons of nitrogen and oxygen in the repeating unit of PNIPAM on the PNIPAM-AuNPs. Taking NP1 as a representative of PNIPAM-AuNPs, an equilibrium constant of association with the $3N^{+}$ fluorophore determined using Stern−Volmer analysis (K_{SV}) was found to be 8.21×10^{8} M^{-1} (Figure S6, Supporting Information).

To ensure that the structures of PNIPAM-AuNPs maintained their physical characteristic throughout the period of protein classification, UV absorption of NP1 and NP2 both before and after $3N^{+}$ addition and after protein addition (BSA was chosen as a representative protein for this set of experiment) was measured. The results shown in Figure S7 (Supporting Information) truly demonstrate that the fluorescence quenching/recovery event happened without causing any changes in the PNIPAM-AuNPs characteristic (shift in absorption

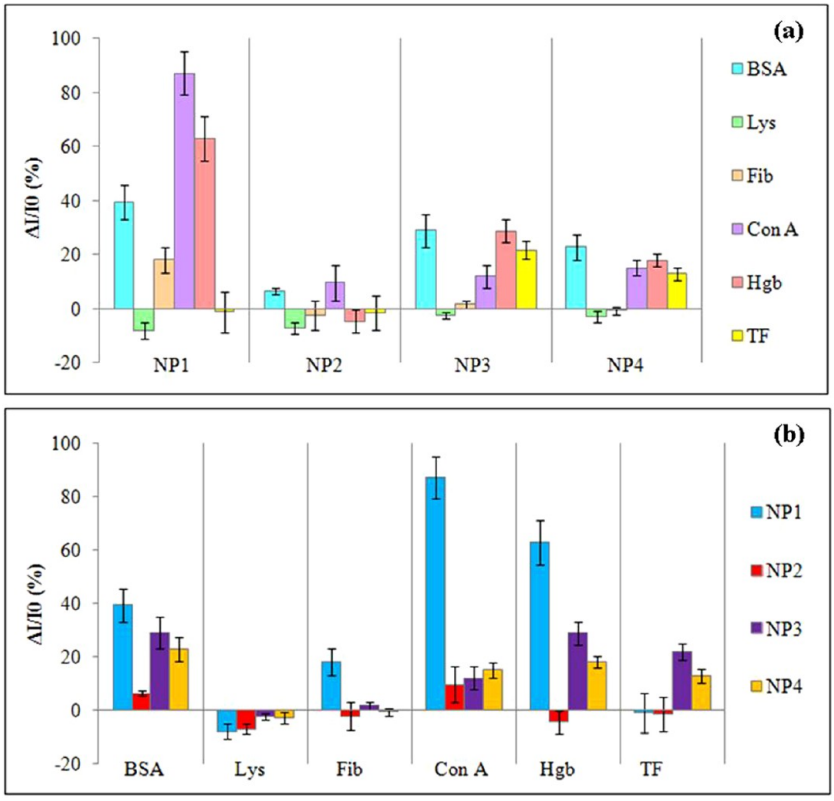

Figure 5. Histogram plot of fluorescence response ($\Delta I/I_0$) patterns of $3N^+$ fluorophore: (a) in the presence of six proteins in PBS for each type PNIPAM-AuNPs and (b) in the presence of PNIPAM-AuNPs for each type of proteins in PBS (responses are averages of six measurements, and error bars are standard deviations).

maximum of surface plasmon band, aggregation). Similar outcome was also observed in the cases of NP3 and NP4 (data not shown).

For the determination of protein based on fluorescence quenching, six types of proteins were analyzed by using NP1-NP4 with the $3N^+$ fluorophore. The obtained results are illustrated in Figure 5a. Each type of PNIPAM-AuNPs exhibited different responses to different proteins. The fluorescence intensities of six proteins in response to NP1 were larger than those in response to other three types of PNIPAM-AuNPs. Unlike NP1, NP2 with its thinner PNIPAM layer may provide stronger interactions with the fluorophore as evidenced by its greater quenching efficiency when compared with NP1 (See Figure S5 in Supporting Information). For this reason, it might be difficult for the fluorophore to be released from NP2 surface upon the protein addition. It is believed that this outcome was influenced by protein resistance property of the PNIPAM brushes which is more prominent at the collapsed state as has been previously described by Xue et al.[44] This may be explained as a result of the collapsed PNIPAM layer of NP2 being denser than that of NP1 so that it is more difficult for the protein to access the fluorophore situated within the PNIPAM layer. That is why the signal responses were lower. In the case of NP3, of which PNIPAM layer was thicker than that of NP1, the change in fluorescence response was proportionally smaller. We explained this as a consequence of the quenching being initially low even before the protein addition due to the long distance between the gold core and the fluorophore. After the addition of protein, the fluorescence signal was not much affected and therefore gave the relatively low response.

Despite the facts that the PNIPAM layer of NP4 was thinner than that of the NP3 and its initial quenching efficiency was as high as that of NP1, overall signal responses of NP4 were relatively small and followed the same trend that observed in the case of NP3. We suspect that the same explanation previously used for NP2 based on limited accessability of the protein to the fluorophore in the condensed layer of PNIPAM can be applied here. In addition, to demonstrate the protein detection profile of the developed sensing array based on four types of PNIPAM-AuNPs, the histogram in Figure 5a was replotted for each protein and shown in Figure 5b. It is obvious that the responsive patterns of AuNPs were varied with the type of protein because of the difference in charge and molecular weight of protein. At pH 7.4, the $3N^+$ fluorophore bound on the AuNPs surface via charge−dipole interactions. Therefore, when the negatively charged proteins (BSA, Fib, Con A, Hgb, and TF) were added, the release of $3N^+$ fluorophore from the AuNPs surface driven by the electrostatic interactions between negatively charged proteins in solution and $3N^+$ fluorophore can take place so that the quenched fluorescence signal can be recovered. Although being negatively charged proteins, Fib and TF did not provide responses against some types of AuNPs. These might be caused by their high molecular weight being obstacle for effective binding with $3N^+$ fluorophore and thus hampering the fluorescence signal recovery. In the case of Lys, a relatively small and positively charged protein, it was found that the signal recovery did not happen. This may be attributed to the repulsive forces between Lys and the $3N^+$ fluorophore. In fact, further quenching was also observed as can be realized from the negative response of the signal. We describe the decrease of fluorescence signal as a

dx.doi.org/10.1021/la402139g | Langmuir 2013, 29, 12317−12327

result of additional quenching of $3N^+$ in the solution that was initially unbound to the PNIPAM-AuNPs. This is likely possible given that it was demonstrated earlier in Figure 4e that the $3N^+$fluorophore was slightly quenched by proteins. The explanation for the impact of characteristic charge and molecular weight of protein on fluorescence signal recovery is schematically summarized in Figure 6.

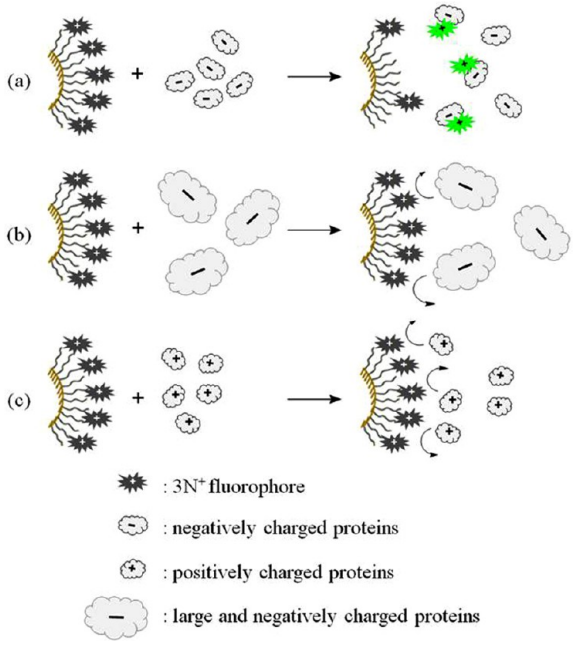

Figure 6. Schematic representation of mechanism explaining the fluorescence signal recovery upon the addition of proteins having different size and charge.

Although the results demonstrated in Figure 5b suggested that the developed sensing platform using the PNIPAM-AuNPs in combination with $3N^+$ fluorophore was applicable for protein identification, the fact that the changes in fluorescence response ($\Delta I/I_0$) determined from the maximum emission intensity independent of the wavelength was not intuitively accurate. Such estimation also ruled out the possibility that the wavelength of the emission maxima may be shifted upon protein addition which was found to be the case in some systems. For more accuracy, the whole spectra obtained before and after adding proteins were taken into consideration when performing subtraction. As can be seen in Figure 7a–d, the subtracted spectra of each protein apparently exhibited different characteristic. The intensity values in wavelength range of 400–600 nm of spectra were used to identify each protein as they show the highest variation of $\%\Delta I$ and the highest shifted λ_{max} toward the proteins. Although the histogram plot and characteristic spectrum already showed different patterns of the fluorescence responses toward each protein analyte, discrimination of these proteins based on this multidimensional data set (4 AuNPs × 6 proteins × 6 replicates) was further simplified using multivariate statistical analyses. In this study, principal component analysis (PCA) was used to transform the data set of fluorescence intensity differences ($\%\Delta I$) into principle component (PC) scores.[45] Based on the data similarity, a two-dimensional PC score plot (PC1 and PC2) suitably generated six clusters on the PC space corresponding to six types of proteins indicating an encouraging level of

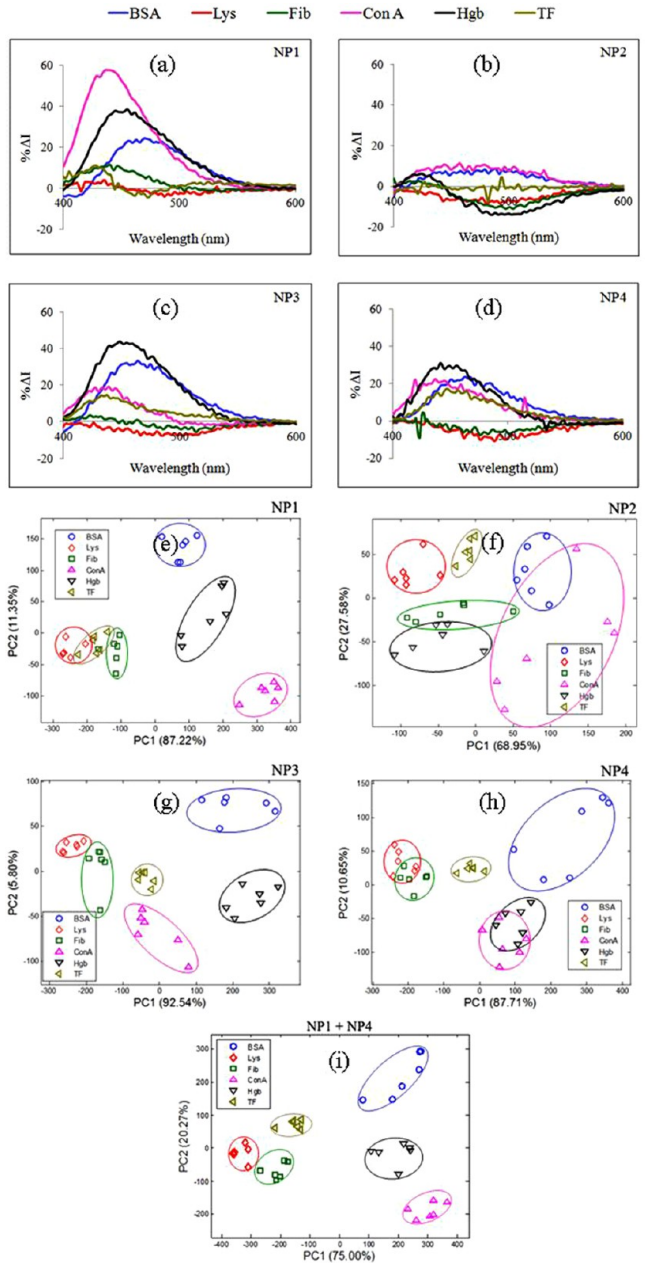

Figure 7. Characteristic emission spectra of $3N^+$ fluorophore in the presence of (a) NP1, (b) NP2, (c) NP3, and (d) NP4 for each type of proteins in PBS (obtained by the subtraction of spectra before and after protein addition) and PCA score plot of $\%\Delta I$ data set obtained from 6 replicates of 6 proteins including fluorescence responses of $3N^+$ fluorophore using (e) NP1, (f) NP2, (g) NP3, (h) NP4, and (i) NP1+NP4.

protein classification (Figure 7e–h). To quantify the classification accuracy, PCA-LDA was applied by performing LDA on the PC scores with a total variance of >95% and then validate the discriminating ability using leave-one-out (LOO) cross validation technique.[34] After PCA-LDA routines were performed on the data by using each type of AuNPs (NP1-NP4), the results showed that the data which used NP3 gave the highest classification accuracy of 97.22%. The obtained data implied that the aggregation of PNIPAM layer induced by thermal treatment (NP2 and NP4) may deteriorate the efficiency of protein classification. However, we found that the 100% of classification accuracy can be obtained by

dx.doi.org/10.1021/la402139g | Langmuir 2013, 29, 12317–12327

combining NP1 data set with NP4 data set. The PCA score plot of NP1 associated with NP4 is shown in Figure 7i. These results strongly indicate the high potential of the developed sensing platform given that proteins can be identified with 100% accuracy by using only two types of PNIPAM-AuNPs.

CONCLUSIONS

This investigation has demonstrated that the thermoresponsive AuNPs can be prepared by using citrate-stabilized AuNPs grafted with PNIPAM-SH synthesized via RAFT polymerization. The prepared PNIPAM-AuNPs have a spherical morphology and uniform size distribution and their shell thickness depended on the PNIPAM-SH molecular weight. Upon molecular weight variation and heat treatment, four types of PNIPAM-AuNPs (NP1-NP4) having different quenching efficiency against $3N^+$ fluorophore were generated. After protein addition, the fluorescence signal of $3N^+$ fluorophore can be recovered. The different pattern of fluorescence signal recovery which is varied with the types of both proteins and PNIPAM-AuNPs can be used to generate an array-based protein classification. Based on LDA analysis using the LOO approach, a 100% accuracy of protein classification can be achieved using a combination of NP1 data set and NP4 data set. The results have suggested that an array-based sensing platform based on chemical nose approach can be developed from PNIPAM-AuNPs when combined with a positively charged phenylene-ethynylene fluorophore.

ASSOCIATED CONTENT

Supporting Information

^{1}H NMR spectra of PNIPAM, UV−vis absorption spectra of PNIPAM and PNIPAM-SH, FTIR spectra of PNIPAM and PNIPAM-AuNPs, amount of grafted PNIPAM chains, particle size of AuNPs obtained from AFM and TEM analysis, physical appearance of PNIPAM-AuNPs solution after two heating cycles upon salt addition, and quenching efficiency of four types of PNIPAM-AuNPs with $3N^+$ fluorophore, zeta potential values of all PNIPAM-AuNPs both before and after $3N^+$ fluorophore addition, K_{SV} plot between $3N^+$ and NP1, and UV−vis absorption spectra of NP1 and NP2 during the process of protein classification. This material is available free of charge via the Internet at http://pubs.acs.org.

AUTHOR INFORMATION

Corresponding Author

*E-mail: vipavee.p@chula.ac.th. Tel: +66-2218-7627. Fax: +66-2218-7598.

Notes

The authors declare no competing financial interest.

ACKNOWLEDGMENTS

This research was financially supported by Chulalongkorn University Centenary Academic Development Project (Under the Center of Innovative Nanotechnology, Chulalongkorn University), the National Research University Project of Thailand, Office of the Higher Education Commission (AM1006A), the Thailand Research Fund (DBG5580003), the Ratchadaphiseksomphot Endowment Fund of Chulalongkorn University (RES560530126-AM), and the Thai Government Stimulus Package 2 (TKK2555), under the Project for Establishment of Comprehensive Center for Innovative Food, Health Products and Agriculture.

REFERENCES

(1) Ishii, T.; Otsuka, H.; Kataoka, K.; Nagasaki, Y. Preparation of functionally PEGylated gold nanoparticles with narrow distribution through autoreduction of auric cation by alpha-biotinyl-PEG-block-[poly(2-(*N*,*N*-dimethylamino)ethyl methacrylate)]. *Langmuir* **2004**, *20* (3), 561−564.

(2) Mirkin, C. A.; Letsinger, R. L.; Mucic, R. C.; Storhoff, J. J. A DNA-based method for rationally assembling nanoparticles into macroscopic materials. *Nature* **1996**, *382* (6592), 607−609.

(3) Storhoff, J. J.; Lazarides, A. A.; Mucic, R. C.; Mirkin, C. A.; Letsinger, R. L.; Schatz, G. C. What controls the optical properties of DNA-linked gold nanoparticle assemblies? *J. Am. Chem. Soc.* **2000**, *122* (19), 4640−4650.

(4) Li, D. X.; He, Q.; Li, J. B. Smart core/shell nanocomposites: Intelligent polymers modified gold nanoparticles. *Adv. Colloid Interface Sci.* **2009**, *149* (1−2), 28−38.

(5) Hussain, I.; Graham, S.; Wang, Z. X.; Tan, B.; Sherrington, D. C.; Rannard, S. P.; Cooper, A. I.; Brust, M. Size-controlled synthesis of near-monodisperse gold nanoparticles in the 1−4 nm range using polymeric stabilizers. *J. Am. Chem. Soc.* **2005**, *127* (47), 16398−16399.

(6) Cui, Y.; Tao, C.; Zheng, S. P.; He, Q.; Ai, S. F.; Li, J. B. Synthesis of thermosensitive PNIPAM-co-MBAA nanotubes by atom transfer radical polymerization within a porous membrane. *Macromol. Rapid Commun.* **2005**, *26* (19), 1552−1556.

(7) Gil, E. S.; Hudson, S. M. Stimuli-reponsive polymers and their bioconjugates. *Prog. Polym. Sci.* **2004**, *29* (12), 1173−1222.

(8) Hu, Z. B.; Chen, Y. Y.; Wang, C. J.; Zheng, Y. D.; Li, Y. Polymer gels with engineered environmentally responsive surface patterns. *Nature* **1998**, *393* (6681), 149−152.

(9) Schilli, C. M.; Zhang, M. F.; Rizzardo, E.; Thang, S. H.; Chong, Y. K.; Edwards, K.; Karlsson, G.; Muller, A. H. E. A new double-responsive block copolymer synthesized via RAFT polymerization: Poly(*N*-isopropylacrylamide)-*block*-poly(acrylic acid). *Macromolecules* **2004**, *37* (21), 7861−7866.

(10) Bohrisch, J.; Wendler, U.; Jaeger, W. Controlled radical polymerization of 4-vinylpyridine. *Macromol. Rapid Commun.* **1997**, *18* (11), 975−982.

(11) Mika, A. M.; Childs, R. F. Acid/base properties of poly(4-vinylpyridine) anchored within microporous membranes. *J. Membr. Sci.* **1999**, *152* (1), 129−140.

(12) Ista, L. K.; Mendez, S.; Perez-Luna, V. H.; Lopez, G. P. Synthesis of poly(*N*-isopropylacrylamide) on initiator-modified self-assembled monolayers. *Langmuir* **2001**, *17* (9), 2552−2555.

(13) Fischer, A.; Brembilla, A.; Lochon, P. Nitroxide-mediated radical polymerization of 4-vinylpyridine: Study of the pseudo-living character of the reaction and influence of temperature and nitroxide concentration. *Macromolecules* **1999**, *32* (19), 6069−6072.

(14) Zhang, J.; Pelton, R. The dynamic behavior of poly(*N*-isopropylacrylamide) at the air/water interface. *Colloids Surf., A* **1999**, *156* (1−3), 111−122.

(15) Wu, C.; Zhou, S. Q. Thermodynamically stable globule state of a single poly(*N*-isopropylacrylamide) chain in water. *Macromolecules* **1995**, *28* (15), 5388−5390.

(16) Wang, X. H.; Wu, C. Light-scattering study of coil-to-globule transition of a poly(*N*-isopropylacrylamide) chain in deuterated water. *Macromolecules* **1999**, *32* (13), 4299−4301.

(17) Kratz, K.; Hellweg, T.; Eimer, W. Structural changes in PNIPAM microgel particles as seen by SANS, DLS, and EM techniques. *Polymer* **2001**, *42* (15), 6631−6639.

(18) Zhu, M. Q.; Wang, L. Q.; Exarhos, G. J.; Li, A. D. Q. Thermosensitive gold nanoparticles. *J. Am. Chem. Soc.* **2004**, *126* (9), 2656−2657.

(19) Yusa, S. I.; Fukuda, K.; Yamamoto, T.; Iwasaki, Y.; Watanabe, A.; Akiyoshi, K.; Morishima, Y. Salt effect on the heat-induced association behavior of gold nanoparticles coated with Poly(*N*-isopropylacrylamide) prepared via reversible addition - Fragmentation chain transfer (RAFT) radical polymerization. *Langmuir* **2007**, *23* (26), 12842−12848.

(20) Shan, J.; Nuopponen, M.; Jiang, H.; Kauppinen, E.; Tenhu, H. Preparation of poly(*N*-isopropylacrylamide)-monolayer-protected gold clusters: Synthesis methods, core size, and thickness of monolayer. *Macromolecules* **2003**, *36* (12), 4526−4533.
(21) Shan, J.; Chen, J.; Nuopponen, M.; Tenhu, H. Two phase transitions of poly(*N*-isopropylacrylamide) brushes bound to gold nanoparticles. *Langmuir* **2004**, *20* (11), 4671−4676.
(22) Chakraborty, S.; Bishnoi, S. W.; Perez-Luna, V. H. Gold nanoparticles with poly(*N*-isopropylacrylamide) formed via surface initiated atom transfer free radical polymerization exhibit unusually slow aggregation kinetics. *J. Phys. Chem. C* **2010**, *114* (13), 5947−5955.
(23) Phillips, R. L.; Miranda, O. R.; You, C. C.; Rotello, V. M.; Bunz, U. H. F. Rapid and efficient identification of bacteria using gold-nanoparticle- Poly(para-phenyleneethynylene) constructs. *Angew. Chem., Int. Ed.* **2008**, *47* (14), 2590−2594.
(24) Miranda, O. R.; Creran, B.; Rotello, V. M. Array-based sensing with nanoparticles: 'Chemical noses' for sensing biomolecules and cell surfaces. *Curr. Opin. Chem. Biol.* **2010**, *14* (6), 728−736.
(25) De, M.; You, C. C.; Srivastava, S.; Rotello, V. M. Biomimetic interactions of proteins with functionalized nanoparticles: A thermodynamic study. *J. Am. Chem. Soc.* **2007**, *129* (35), 10747−10753.
(26) De, M.; Rana, S.; Akpinar, H.; Miranda, O. R.; Arvizo, R. R.; Bunz, U. H. F.; Rotello, V. M. Sensing of proteins in human serum using conjugates of nanoparticles and green fluorescent protein. *Nat. Chem.* **2009**, *1* (6), 461−465.
(27) Schilli, C.; Lanzendorfer, M. G.; Muller, A. H. E. Benzyl and cumyl dithiocarbamates as chain transfer agent in the RAFT polymerization of *N*-isopropylacrylamide. In situ FT-NIR and MALDI-TOF MS investigation. *Macromolecules* **2002**, *35* (18), 6819−6827.
(28) Ray, B.; Isobe, Y.; Morioka, K.; Habaue, S.; Okamoto, Y.; Kamigaito, M.; Sawamoto, M. Synthesis of isotactic poly(*N*-isopropylacrylamide) by RAFT polymerization in the presence of Lewis acid. *Macromolecules* **2003**, *36* (3), 543−545.
(29) Kujawa, P.; Segui, F.; Shaban, S.; Diab, C.; Okada, Y.; Tanaka, F.; Winnik, F. M. Impact of end-group association and main-chain hydration on the thermosensitive properties of hydrophobically modified telechelic poly(*N*-isopropylacrylamides) in water. *Macromolecules* **2006**, *39* (1), 341−348.
(30) Ganachaud, F.; Monteiro, M. J.; Gilbert, R. G.; Dourges, M. A.; Thang, S. H.; Rizzardo, E. Molecular weight characterization of poly(*N*-isopropylacrylamide) prepared by living free-radical polymerization. *Macromolecules* **2000**, *33* (18), 6738−6745.
(31) Convertine, A. J.; Ayres, N.; Scales, C. W.; Lowe, A. B.; McCormick, C. L. Facile, controlled, room-temperature RAFT polymerization of *N*-isopropylacrylamide. *Biomacromolecules* **2004**, *5* (4), 1177−1180.
(32) Niamnont, N.; Mungkarndee, R.; Techakriengkrai, I.; Rashatasakhon, P.; Sukwattanasinitt, M. Protein discrimination by fluorescent sensor array constituted of variously charged dendritic phenylene-ethynylene fluorophores. *Biosens. Bioelectron.* **2010**, *26* (2), 863−867.
(33) Hayat, A. Colloidal gold: principles, methods, and applications. *J. Anat.* **1989**, *176*, 215−216.
(34) Brereton, R. G. *Chemometrics for pattern recognition*; Wiley & Sons: Chichester, 2009.
(35) Varmuza, K. *Chemometrics in practical applications*; InTech publisher: Rijeka, 2012.
(36) Lloyd, G. R.; Orr, L. E.; Christie-Brown, J.; McCarthy, K.; Rose, S.; Thomas, M.; Stone, N. Discrimination between benign, primary and secondary malignancies in lymph nodes from the head and neck utilising Raman spectroscopy and multivariate analysis. *Analyst* **2013**, *138* (14), 3900−3908.
(37) Smit, S.; van Breemen, M. J.; Hoefsloot, H. C. J.; Smilde, A. K.; Aerts, J. M. F. G. de Koster, C. G. Assessing the statistical validity of proteomics based biomarkers. *Anal. Chim. Acta* **2007**, *592* (2), 210−217.
(38) van der Werf, M. J.; Pieterse, B.; van Luijk, N.; Schuren, F.; van der Werff-van der Vat, B.; Overkamp, K.; Jellema, R. H. Multivariate analysis of microarray data by principal component discriminant analysis: prioritizing relevant transcripts linked to the degradation of different carbohydrates in *Pseudomonas putida* S12. *Microbiology* **2006**, *152*, 257−272.
(39) Nakayama, M.; Okano, T. Polymer terminal group effects on properties of thermoresponsive polymeric micelles with controlled outer-shell chain lengths. *Biomacromolecules* **2005**, *6* (4), 2320−2327.
(40) Andersson, M.; Hietala, S.; Tenhu, H.; Maunu, S. L. Polystyrene latex particles coated with crosslinked poly(*N*-isopropylacrylamide). *Colloid Polym. Sci.* **2006**, *284* (11), 1255−1263.
(41) Chen, Q.; Xu, K.; Zhang, W. D.; Song, C. L.; Wang, P. X. Preparation and characterization of poly (*N*-isopropylacrylamide)/polyvinylamine core-shell microgels. *Colloid Polym. Sci.* **2009**, *287* (11), 1339−1346.
(42) Scales, C. W.; Convertine, A. J.; McCormick, C. L. Room-temperature polymerization of *N*-isopropylacrylamide via RAFT and subsequent conjugation of fluorescent labels. *Abstr. Pap. Am. Chem. Soc.* **2005**, *230*, U4233−U4234.
(43) Du, B. Y.; Mei, A. X.; Tao, P. J.; Zhao, B.; Cao, Z.; Nie, J. J.; Xu, J. T.; Fan, Z. Q. Poly[*N*-isopropylacrylamide-*co*-3-(trimethoxysilyl)-propylmethacrylate] coated aqueous dispersed thermosensitive Fe_3O_4 nanoparticles. *J. Phys. Chem. C* **2009**, *113* (23), 10090−10096.
(44) Xue, C. Y.; Yonet-Tanyeri, N.; Brouette, N.; Sferrazza, M.; Braun, P. V.; Leckband, D. E. Protein adsorption on poly(*N*-isopropylacrylamide) brushes: dependence on grafting density and chain collapse. *Langmuir* **2011**, *27* (14), 8810−8818.
(45) Poulli, K. I.; Mousdis, G. A.; Georgiou, C. A. Classification of edible and lampante virgin olive oil based on synchronous fluorescence and total luminescence spectroscopy. *Anal. Chim. Acta* **2005**, *542* (2), 151−156.